3D shear-mode fatigue crack growth in maraging steel

V. Doquet[1], Q.H. Bui[1], L. Alves[1], G. Bertolino[2]

[1] LMS, CNRS, Ecole Polytechnique, 91128 Palaiseau cedex, France
doquet@lms.polytechnique.fr
[2] CONICET, Centro Atomico Bariloche – Argentina, bertolin@cab.cnea.gov.ar

ABSTRACT. *Fatigue crack growth tests in mixed-mode II + III were performed on maraging steel using an assymmetric four point bending device and the 3D evolutions of the crack fronts -measured by SEM after interrupted tests- were analyzed, taking into account the reduction in effective crack driving force by the interlocking and friction of the asperities of the crack surface. The crack growth rates were found to correlate best with* $\sqrt{\Delta K_{II}^{eff\,2} + 1.2\Delta K_{III}^{eff\,2}}$.

INTRODUCTION.

Mode II and mode III fatigue crack growth are generally studied separately, using different setups. However, crack growth has to be envisaged in 3D, as in real engineering problems. In rolling contact fatigue, elliptical cracks initiated on subsurface defects grow in mode II+III with a variable K_{II}/K_{III} along their front. This is also the case for surface cracks in torsion fatigue. Mixed-mode threshold and kinetics are needed to predict their evolution. But to the authors best knowledge, only Hellier et al [1] Murakami et al [2] and Pokluda et al [3,4] tried to obtain such mixed-mode data or at least mode II and III data on the same material, for comparison. Pokluda et al. concluded that mode III crack growth is slower than mode II when $\Delta K_{II}=\Delta K_{III}$. Conversely, Murakami et al. concluded that the mechanisms and thresholds for mode II and mode III were essentially the same. Hellier and Corderoy developed an assymmetrical 4 points bending device in which a specimen with an edge notch can be turned around a horizontal axis so as to vary continuously K_{II}/K_{III} from zero to infinity, at least in principle, since 3D finite element computations reported below show that pure mode II or III cannot be obtained, except at mid-thickness. This device is however interesting, provided the gradient in mode-mixity along the front is taken into account. A similar device was thus built and used to investigate mixed-mode fatigue II +III crack growth in Ti-6Al-4V, in a previous study and in maraging steel, in the present work.

EXPERIMENTAL AND NUMERICAL PROCEDURES.

An asymmetrical 4 points bending device in which the specimen can be turned around a horizontal axis by an angle α has been built (fig. 1). The assymmetry is such that only a shearing force and no bending moment are applied in the cracked section.

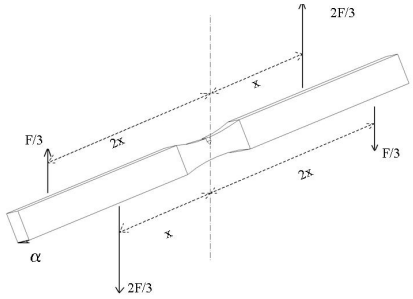

Figure 1: Principle of assymmetrical 4 points bending tests

The maraging steel investigated has a very high yield stress ($R_{p0.2}$≈1720MPa) but low hardening capacity ($R_m/R_{p0.2}$≈1.03). Specimens with a 10*10mm central section and a 3.5mm-deep edge notch were used. Mode I fatigue precracking over 1 to 1,5mm was performed in symmetrical 4 points bending with ΔK_I smaller than 15MPa√m. Fully reversed bending tests were then performed at a low frequency (0.05Hz) for various loading ranges and inclination of the precrack front relative to the horizontal. The tests were interrupted after a small number of cycles. Mode I fatigue was then resumed until fracture. The shapes and positions of the slightly tunneling precrack front and of the final crack front at the end of shear-mode loading were determined by SEM fractographic observations. The test conditions are specified in Table 1.

Table 1: Test conditions. α denotes the angle between the crack front and horizontal

Test number	α	Loading range	Number of cycles	Coplanar crack growth on free surfaces
5	0°	±35KN	500	400 and 430µm
7	0°	±38KN	350	800 and 725µm
2	15°	±35KN	1500	1000 and 60µm
1	30°	±35KN	500	565 and 0µm
3	45°	±35KN	500	840 and 30µm
4	60°	±35KN	500	800 and 0µm
6	75°	±35KN	1500	2330 and 90µm
9	90°	±25KN	600	310 and 50µm
11	90°	±32KN	500	300 and 310µm
12	90°	±35KN	500	430 and 375µm
10	90°	±38KN	350	360 and 765µm

The tests were periodically interrupted for preparation of plastic replicas at minimum and maximum load, from which positive replicas were cast, which allowed SEM observations of cracks, as well as measurements of both the in-plane and out-of-plane crack face relative sliding displacements associated with mode II and III, respectively. For the former, two parallel rows of microhardness indents, 50µm above and below the precrack were used to measure, on high resolution SEM images, the discontinuity of in-plane sliding displacements across the crack, at maximum and minimum load, as a function of the distance to the crack tip. For the latter, optical chromatic confocal microscopy was used to measure the topography of pairs of positive replicas taken at maximum and minimum load, with a 0.3µm precision on height. The discontinuities in z across the crack correspond to the relative out-of-plane sliding displacements. To evaluate the ratios $U_{II} = \frac{\Delta K_{II}^{effective}}{\Delta K_{II}^{nominal}}$ and $U_{III} = \frac{\Delta K_{III}^{effective}}{\Delta K_{III}^{nominal}}$, the measured displacements were compared to those issued from elastic-plastic F.E. computations performed for a smooth, frictionless crack. For that purpose, constitutive equations with isotropic and non-linear kinematic hardening fitted to experimental stress-strain curves measured in tension and push-pull were used. Such computations are necessary, because as illustrated on Fig. 2, elastic computations would underestimate the expected displacements for a smooth frictionless crack, at high ΔK_{II} or ΔK_{III}. U_{II} and U_{III}, averaged over a distance of 1mm from the crack tip, were found to be approximately the same and will be simply denoted by U.

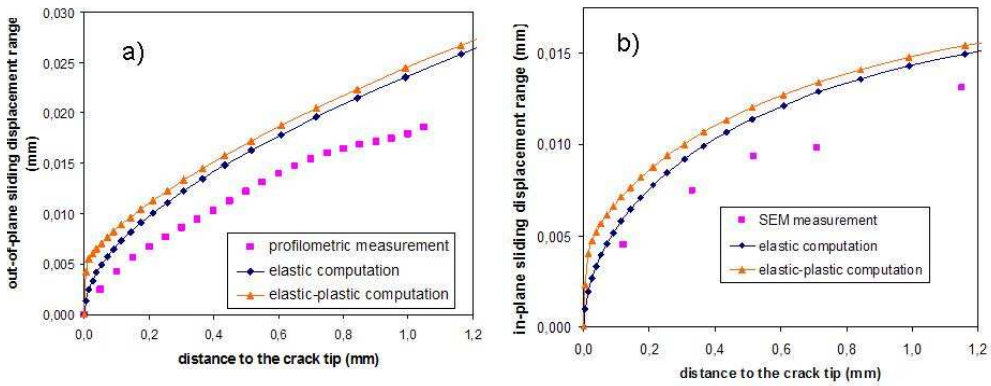

Figure 2: Comparison of measured and computed a) in-plane and b) out-of-plane sliding displacement ranges (test n°9)

The topography of fracture surfaces was measured using confocal microscopy and the absence of significant tilt or twist, which would reveal bifurcation towards mode I could be checked. Data from areas with tilt or twist angles larger than ±12° were discarded. Only coplanar shear-mode crack growth is thus analyzed below.

Polynomial fits of the distance to the notch root of the precrack and final crack front as a function of depth y, $a_0(y)$ and $a_f(y)$ were obtained. The local crack length increment during N shear-mode cycles was computed as $\Delta a(y) = a_f(y) - a_0(y)$ and, considering the

small number of applied cycles, the local growth rate was approximated as: $\frac{da}{dN}(y) \approx \frac{\Delta a(y)}{N}$. The main purpose of the study was to determine how these local growth rates correlate with the local stress intensity factors, $\Delta K_{II}(y)$ and $\Delta K_{III}(y)$ after appropriate corrections for friction effects.

A 3D finite element model of specimens was prepared, with a refined mesh around the crack front (Fig. 3). The applied load, F, splitted into F/3 and 2F/3 (because of the asymmetrical position of the support and loading rings) was distributed uniformly over each contact area. When the inclination angle α of the crack plane relative to the horizontal axis was neither zero nor 90°, the reactions on the two side faces of the specimens in contact with the loading rings were supposed to be proportional to $\cos(\alpha)$ and $\sin(\alpha)$. The stress intensity factors were obtained by a perturbation method (G-theta) after elastic computations. Due to corner point singularities, the values computed at the two external nodes on the side surfaces were not included in the plots below. Figure 4 shows the profiles of stress intensity factors along the crack front computed for α=0, 90 and 45°, for an applied load of 35KN.

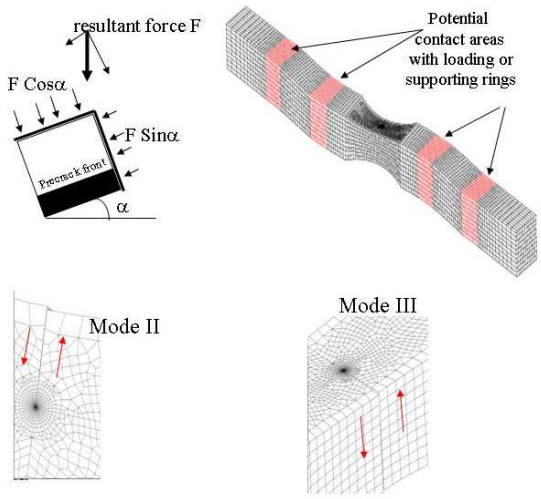

Figure 3: Finite element model of bending specimens

For α=0°, pure mode II is found at mid-thickness only, since a skew-symmetric mode III component is superimposed. Near the surface, K_{III} reaches approximately 30% of K_{II}. Similarly, for α=90°, pure mode III is found at mid-thickness only, since a skew-symmetric mode II is superimposed. However, the coupling is much stronger in that case, since K_{II} is as large as K_{III} near the surface. For any other angle different from 0 and 90°, K_{II}, K_{III} and G all have an assymmetrical profile. Mixed-mode II + III is found along the whole crack front and the mode mixity ratio $\Delta K_{II}/\Delta K_{III}$ varies between 0.5 and 2 from one side to the other.

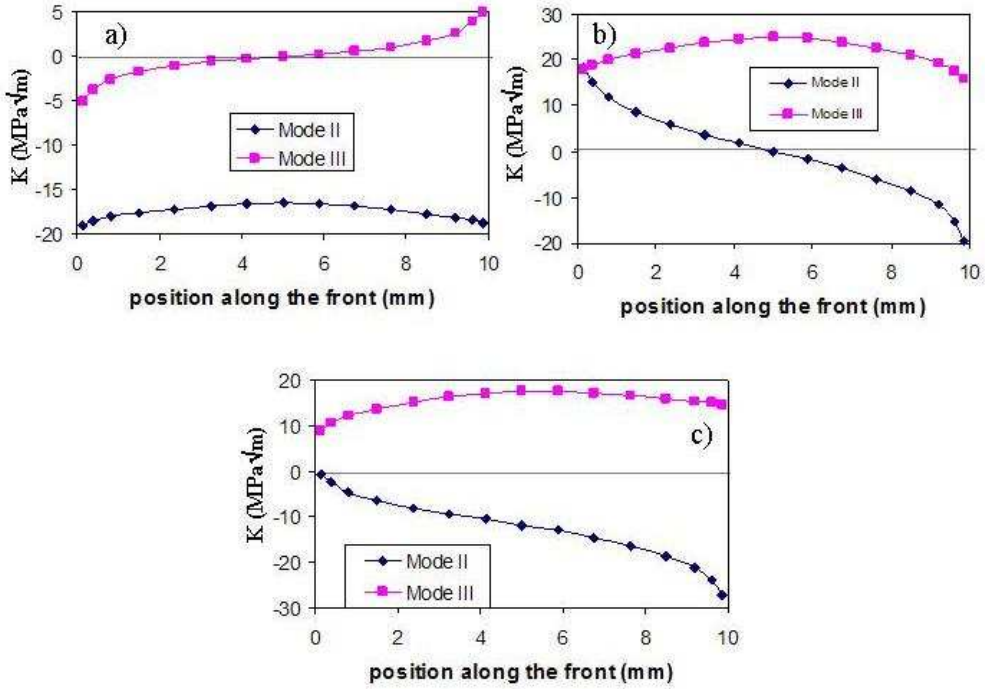

Figure 4: Profiles of K_{II}, K_{III} along the crack front for a) α=0°, b) α=90° and c) α= 45°

RESULTS AND ANALYSIS

Fig. 5, 6 and 7 show the fracture surfaces for tests n°7, 10 and 3, respectively.

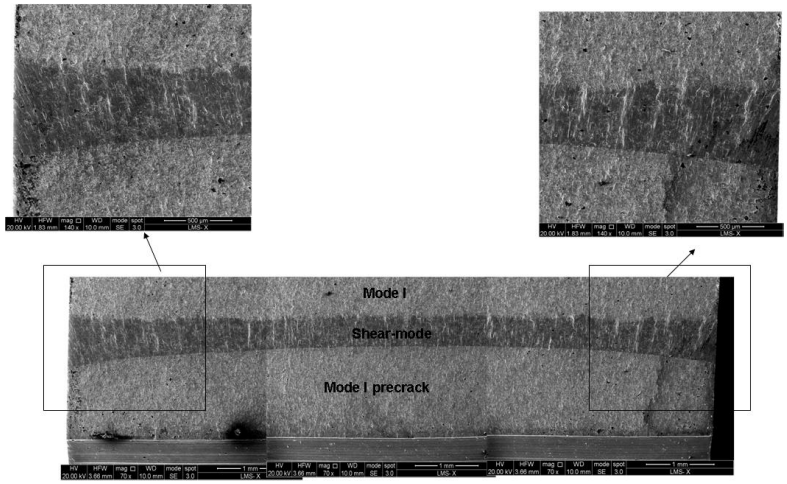

Figure 5: Fracture surface of specimen 7 (α=0°)

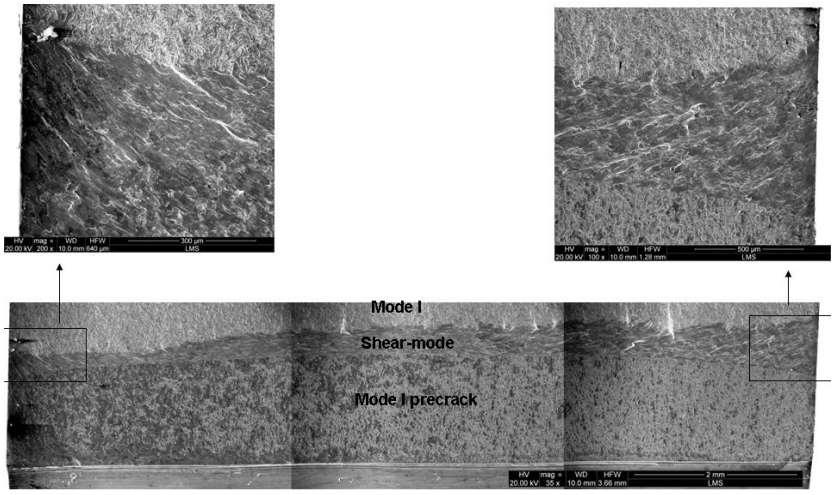

Figure 6: Fracture surfaces of specimen n°10 (α=90°)

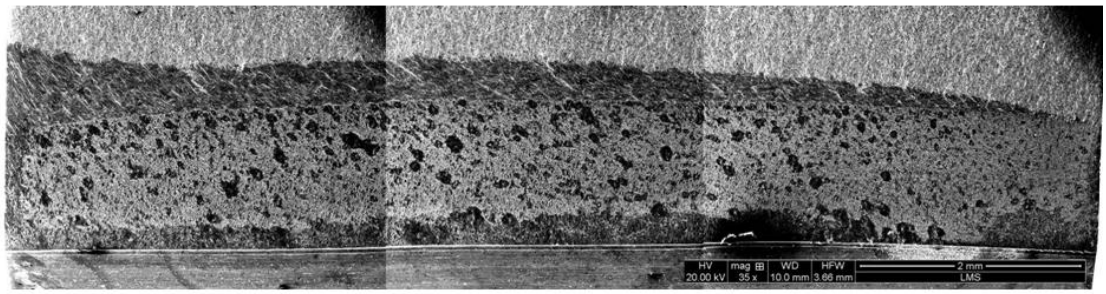

Figure 7: Fracture surfaces of specimen n°9 (α=45°)

All fracture surfaces were heavily worn. The orientation of wear scars, which gives the direction of local sliding displacements (parallel to the precrack front at mid-thickness, for test n°10, but inclined by ±45°near free surfaces, perpendicular to the precrack front at mid-thickness, for test n°7, but inclined by ±17°near free surfaces) was coherent with the computed profile of the mode-mixity-ratio $\Delta K_{II}/\Delta K_{III}$. When the precrack front was neither horizontal nor vertical, a large assymmetry in the crack development was observed. The measured $U = \frac{\Delta K^{\text{effective}}}{\Delta K^{\text{nominal}}}$ are reported in Table 2.

Table 2: Ratio of effective to nominal stress intensity factors for maraging steel

Test	7 0°	2 15°	1 30°	3 45°	4 60°	6 75°	9 90°	11 90°	12 90°	10 90°
U	1.0	0.57	0.62	0.65	0.65	0.59	0.67	0.66	0.57	0.51

These values are comparable to those measured previously in Mode II on CTS or tubular specimens [5, 6]. Searching for the most suitable Paris-type correlation of measured crack growth rates of the form:

$$\frac{da}{dN} = C\sqrt{\Delta K_{II}^{eff\,2} + \beta \Delta K_{III}^{eff\,2}}^{\,n} \qquad (3)$$

values of β ranging from 0 - corresponding to ΔK_{II}-driven crack growth- to 1/(1-ν) (≈1.43) – corresponding to ΔG-driven crack growth- were tried. Figure 8a shows the evolution of the correlation coefficient of the fits, as a function of β and Fig. 8b the corresponding best fit. The optimum β appears to be 1.2 and the corresponding exponent, n = 3.5. Data from a previous study [5] concerning mode II fatigue crack growth in maraging steel CTS or tubular specimens were also plotted. A satisfactory agreement with the best fit of kinetic data from the present study is observed.

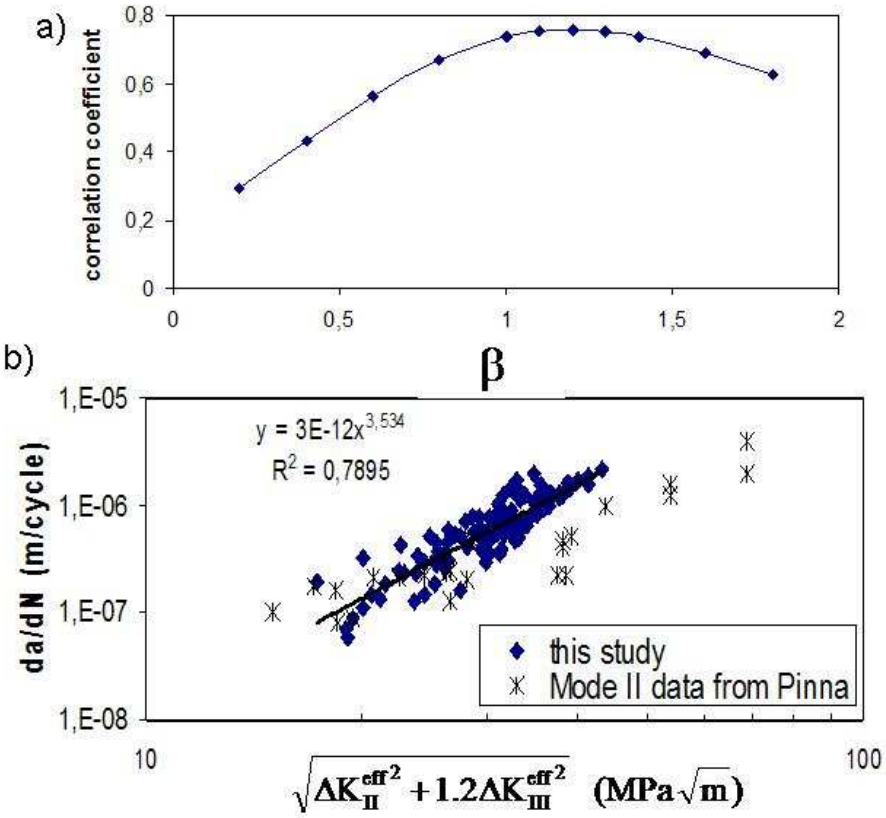

Figure 8: Correlation of kinetic data. a) determination of the best value for β and b) best correlation of kinetic data

CONCLUSIONS

Fatigue crack growth tests in mixed-mode II + III were performed on maraging steel and the 3D evolutions of the crack fronts were analyzed taking into account the reduction in effective crack driving force by the interlocking and friction of the asperities of the crack surface.The crack growth rates were found to correlate best with $\sqrt{\Delta K_{II}^{eff\,2} + 1.2\Delta K_{III}^{eff\,2}}$.

REFERENCES

[1] Hellier A.K., Corderoy D.J.H., McGirr M.B. (1987), *Int. Journ. Fatigue*, **9**, 95-101

[2] Murakami Y, Kusumoto R, Takahashi K (2002), *Proc. 14th European Conf. Fracture*, Cracow, Poland 8-13 Sept., Vol. 2, 493-500, Ed: A Neimitz, I.V. Rokach, D Kocanda, K Golos, EMAS books

[3] Pokluda J, Trattnig G, Martinschitz C, Pippan R (2008), *Int. Journ. Fatigue* **30**, 1498-1506

[4] Holáň L, Pippan R, Pokluda J, Horníková J, Hohenwarter A, Slámečka K (2009) *Int. Conf. on Crack Paths*, Vicenza, Italy, 25-29 Sept.

[5] Pinna C, Doquet V (1999), *Fatigue Fract. Engng. Mater. Struct*. **22**:173-183

[6] Doquet V, Bertolino G (2008) *Engng. Fracture Mech.* **75**:3399-3412